ParisTech
INSTITUT DES SCIENCES ET TECHNOLOGIES
PARIS INSTITUTE OF TECHNOLOGY

MINES ParisTech

École doctorale nº 364 : Sciences Fondamentales et Appliquées

Doctorat ParisTech

T H È S E

pour obtenir le grade de docteur délivré par

l'École Nationale Supérieure des Mines de Paris

Spécialité doctorale "Science et Génie des Matériaux"

présentée et soutenue publiquement par

Ali SAAD

le xx mai 2015

NUMERICAL MODELLING OF MACROSEGREGATION INDUCED BY SOLIDIFICATION SHRINKAGE IN A LEVEL SET APPROACH

Directeurs de thèse: **Michel BELLET**
Charles-André GANDIN

Jury

M. Blablabla,	Professeur, MINES ParisTech	Rapporteur
M. Blablabla,	Professeur, Arts Et Métiers ParisTech	Rapporteur
M. Blablabla,	Chargé de recherche, ENS Cachan	Examinateur
M. Blablabla,	Danseuse, en freelance	Examinateur
M. Blablabla,	Ingénieur, MIT	Examinateur

MINES ParisTech
Centre de Mise Forme des Matériaux (CEMEF)
UMR CNRS 7635, F-06904 Sophia Antipolis, France

T H E S E

Contents

1 Energy balance with thermodynamic tabulations **1**
1.1 State of the art . . . 2
1.2 Thermodynamic considerations . . . 2
1.2.1 Volume averaging . . . 2
1.2.2 The temperature-enthalpy relationship . . . 3
1.2.3 Tabulation of properties . . . 4
1.3 Numerical method . . . 5
1.3.1 Enthalpy-based approach . . . 7
1.3.2 Temperature-based approach . . . 8
1.3.3 Convergence . . . 8
1.4 Validation . . . 10
1.4.1 Pure diffusion . . . 10
1.4.2 Convection-diffusion with macrosegregation . . . 13

Bibliography **17**

Acronym	Standing for
ALE	Arbitrary Lagrangian-Eulerian
CCEMLCC	Chill Cooling for the Electro-Magnetic Levitator in relation with Continuous Casting of steel
CEMEF	Center for Material Forming
DLR	Deutsches Zentrum für Luft- und Raumfahrt
EML	Electromagnetic levitation
ESA	European Space Agency
FEM	Finite Element Method
ISS	International Space Station
IWT	Institut für Werkstofftechnik
LHS	Left Hand Side
MAC	Marker-and-cell
PF	Phase field
RHS	Right Hand Side
RUB	Ruhr Universität Bochum
RVE	Representative Elementary Volume
VOF	Volume Of Fluid

Chapter 1

Energy balance with thermodynamic tabulations

Contents

1.1 State of the art 2
1.2 Thermodynamic considerations 2
1.2.1 Volume averaging 2
1.2.2 The temperature-enthalpy relationship 3
1.2.3 Tabulation of properties 4
1.3 Numerical method 5
1.3.1 Enthalpy-based approach 7
1.3.2 Temperature-based approach 8
1.3.3 Convergence 8
1.4 Validation 10
1.4.1 Pure diffusion 10
1.4.2 Convection-diffusion with macrosegregation 13

1.1 State of the art

Use of enthalpy resolution in the majority of works
motivation and advantages of TvsH without talking about resolution time
use article's introduction to fill this section (or improvise new things)

When speaking about macrosegregation, one needs to know that the problem involves phase change. For that, a minimum of four conservation equations are necessary: conservation of mass, momentum, chemical species and energy. The phase change literature contains a wealth of numerical methods to solve energy conservation in solidifying alloys. A comprehensive overview of these methods is given by Swaminathan. et al. [1993]. The corresponding equation associates the total average enthalpy to the temperature via intrinsic alloy properties, such as the heat capacity of the phases and the latent heat associated with the phase transformations. However, in the course of solidification and while macrosegregation is taking place, these properties may change because the average composition may vary significantly: the transformation paths are thus modified, as well as the phases' composition and heat capacity. Similarly, the latent heat of phase transformations is not a mere constant that could be distributed as a function of the phase fractions assuming only temperature-dependent phases' properties, as often found in the literature [Bellet et al. 2009]. It is thus impossible to establish a priori the dependence of the enthalpy with respect to temperature when macrosegregation takes place, even in the case of full thermodynamic equilibrium between phases. In this chapter, we discuss a suitable numerical scheme based on an enthalpy method, already used in the literature to alleviate this macrosegregation-related problem [Swaminathan. et al. 1993; Carozzani et al. 2013]. Later on, we introduce a modified formulation, using the effective heat capacity method that increases the original scheme's efficiency.
The current method is thus an enthalpy method that makes use of a temperature-based solver. Moreover, it uses tabulated thermodynamic quantities (solidification paths, phases' enthalpy and composition) in a range of average compositions and temperatures as found in the literature [Doré et al. 2000; Thuinet et al. 2004; Du et al. 2007], with the aim of evaluating the total average enthalpy as well as the effective heat capacity. The novelty of the modified method resides in the use of thermodynamic tabulations without losing the advantages of the previous method, thus yielding faster computation times while maintaining a good accuracy.

1.2 Thermodynamic considerations

1.2.1 Volume averaging

the following paragraph will be deleted once the volume averaging has been introduced in chapter 1

A volume averaging technique was suggested to deal with the presence of multiple

phases [Ni et al. 1991]. It locally considers a Representative Volume Element (RVE) that contains a single or several phases (these are not necessarily in thermodynamic equilibrium) at a mesoscopic scale. We represent, for each unknown ψ, an intrinsic volume average, $\langle\psi\rangle^\phi$ (also denoted $\langle\psi^\phi\rangle^\phi$ in the literature), corresponding to a phase ϕ. The volume average $\langle\psi\rangle$ for this unknown in the RVE, hence averaged over all the present phases writes:

$$\langle\psi\rangle = \sum_\phi g^\phi \langle\psi\rangle^\phi \tag{1.1}$$

where g^ϕ denotes the volume fraction of phase ϕ in the RVE. It should be emphasized that the averaging technique applies to virtually all thermodynamic variables (enthalpy, density ...). Among these variables, the temperature is also considered to be uniform in the RVE. Applying the volume averaging technique to the energy conservation principle along with interfacial balances between the phases, results in the following averaged equation [Rappaz et al. 2003]:

$$\frac{\partial\langle\rho h\rangle}{\partial t} + \vec{\nabla}\cdot\langle\rho h\vec{v}\rangle = \vec{\nabla}\cdot\left(\langle\kappa\rangle\vec{\nabla}T\right) + \langle\dot{Q}_V\rangle \tag{1.2}$$

where ρ stands for the density, h the mass enthalpy, $\vec{v}$ the velocity field, κ the thermal conductivity, T the temperature and $\dot{Q}_V$ a possible volume heat source. Equation (1.2) is the standard averaged form of the energy conservation equation used in non-stationary phase change problems.

I could elaborate more in this paragraph by showing the possible equations for the explicit formulation and maybe a figure to show the AlSi7 computation that i did with a v small time step

Once the variational form has been discretized in space and time, two possible resolution schemes emerge: the first is an explicit forward Euler scheme which gives rise to a linear equation where the temperature is known at time t, T^t. This requires very small time steps in the current context, which limits the solver's usability at the scale of industrial applications. The second scheme is the backward Euler or full implicit discretization where terms are function of $T^{t+\Delta t}$. It leads to a nonlinear equation with 2 interdependent unknowns, $\langle\rho h\rangle^{t+\Delta t}$ and $T^{t+\Delta t}$. It is clear that the nature of the temperature-enthalpy relationship plays a central role when formulating the resolution strategy of this nonlinear equation. Generally, it is admitted that, depending on the resolution strategy, it is necessary to express enthalpy as a function of temperature or vice-versa, together with associated partial derivatives, $\frac{d\langle\rho h\rangle}{dT}$ or $\frac{dT}{d\langle\rho h\rangle}$.

1.2.2 The temperature-enthalpy relationship

In solidification problems, additional variables are involved in eq. (1.1) and eq. (1.2), like the transformation path that defines the history of the phase fractions, as well as the average chemical composition $\langle w_i\rangle$, i being the index of the chemical species

(only the solutes are considered). The temperature-enthalpy relation averaged over the phases in a given RVE writes:

$$\langle \rho h \rangle = \sum_{\phi} g^{\phi}{}_{(T,\langle w_i \rangle \ldots)} \rho^{\phi}_{\left(T,\langle w_i \rangle^{\phi} \ldots\right)} h^{\phi}_{\left(T,\langle w_i \rangle^{\phi} \ldots\right)} \tag{1.3}$$

Note that the volume average enthalpy is approximated by the product $\langle \rho h \rangle^{\phi} = \langle \rho \rangle^{\phi} \langle h \rangle^{\phi}$ in the current work. As stated in the introduction, it becomes clear from eq. (1.3) that phase properties, i.e. average phase density, , $\rho^{\phi}$and enthalpy, h^{ϕ}, are temperature and composition dependent. This equation is the key to convert the average volume enthalpy to temperature (through a procedure named *H2T*) or vice-versa (*T2H*). The values of the different phase fractions g^{ϕ} (solidification path) and phase enthalpies $\langle \rho h \rangle^{\phi}$ are thus needed to close the relation.

1.2.3 Tabulation of properties

The complexity of performing a thermodynamic conversion is directly linked to the simplicity of determining the alloy properties, namely the phase fractions and phase enthalpies. In the case of binary alloys and with several assumptions with respect to the system (e.g., linear monovariant temperature composition relationships, constant heat capacity of phases and constant latent heat of transformations, equilibrium approximations between phases) analytical calculations are often used to determine the properties. Nevertheless, analytical relations are more complex or even impossible to derive in the case of multicomponent alloys ($i > 1$). To overcome this problem, one can resort to thermodynamic databases and phase equilibrium calculations to tabulate the transformation paths and the phase enthalpies for a given range of temperatures and average compositions. It is a handy solution for two main reasons: first, the conversion is merely a binary search in a table; secondly, it is a simple solution for coupling with macrosegregation. In this way, phase fractions g^{ϕ} are tabulated as functions of temperature and average composition, while for each phase ϕ the mass enthalpy, h^{ϕ}, and the density, ρ^{ϕ}, are tabulated as functions of temperature and phase intrinsic average compositions $\langle w_i \rangle^{\phi}$, as well as other possible parameters. Table 1.1 summarizes the steps in order to perform a temperature-to-enthalpy (*T2H*) conversion using the predefined tabulation approach. In step 1, the transformation path is acquired for each average composition and temperature to determine the list of phases, their volume fractions g^{ϕ} and their intrinsic compositions $\langle w_i \rangle^{\phi}$. In step 2, the phase enthalpy h^{ϕ} and density ρ^{ϕ} are determined by searching for the temperature and the already known phase composition $\langle w_i \rangle^{\phi}$. In step 3, the average volume enthalpy is computed from the volume fraction, density and mass enthalpy of phases using eq. (1.3). The methodology to build the tabulations is straightforward. It is based on two main scans. On the one hand, intervals for the variation of the average composition $\langle w_i \rangle$ are chosen from the known alloy composition. These variations have to cover the extreme values adopted during the simulation, which are not known a

Table 1.1 – Tabulation processing for a *T2H* procedure

Step Number	**1**	**2**	**3**
Inputs	$T, \langle w_i \rangle$	$T, \langle w_i \rangle^{\phi}$	$g^{\phi}, \rho^{\phi} h^{\phi}$
Outputs	$g^{\phi}, \langle w_i \rangle^{\phi}$	ρ^{ϕ}, h^{ϕ}	$\langle \rho h \rangle$ (eq. (1.3))

priori. An interval is also selected for the variation of temperature. The latter is easier to determine as it usually starts from the initial melt temperature and goes down to the room temperature in a standard casting simulation. For these intervals, a systematic scan is made with chosen steps in each composition and T, during which a thermodynamic equilibrium is computed. The outputs are the number of phases encountered, together with their fraction and intrinsic composition. The minimum and maximum intrinsic composition for each phase could then be determined. On the other hand, for each phase, a scan of the intrinsic composition and temperature is made to compute the intrinsic properties. The same temperature interval and step as defined earlier are used.

below paragraph should be re written and maybe stress LESS on the speed effect

I should change the superscript k which may be confused with partition coefficient

Regarding the enthalpy-to-temperature conversion (*H2T*), a backward iterative *T2H* search is performed. For a known composition $\langle w_i \rangle$, denoting k the iteration index to convert the enthalpy $\langle \rho h \rangle_{\text{input}}$, we start with an initial guess for temperature $T^{(k=0)}$ then convert it to an enthalpy $\langle \rho h \rangle^{(k=0)}$ with the *T2H* conversion. Using an appropriate nonlinear algorithm (Brent is the most versatile in our case), we aim at minimizing the following residual: $\text{Residu}_{\langle \rho h \rangle} = \left| \langle \rho h \rangle_{\text{input}} - \langle \rho h \rangle^{(k)} \right|$. Once the algorithm has converged, the temperature $T^{(\nu)}$ is the result of the *H2T* conversion. It is inferred that the first conversion (*T2H*) is a direct one whereas the latter (*H2T*) is indirect and requires a series of iterative steps; each step being a single *T2H* resolution. In other words, a *H2T* conversion is a backward search for a temperature, hence it's slower. This conversion's speed lag is exacerbated when tabulations increase in size (e.g. large number of temperature and composition steps) and complexity (e.g., multicomponent industrial alloys used in casting), since the search gets more complicated with the increasing number of input columns (one column for each alloying element).

1.3 Numerical method

The finite element method is used to solve the energy conservation as expressed by eq. (1.2). A test function $\mathcal{W}$ belonging to the Hilbertian Sobolev space $\mathcal{H}^1(\Omega)$ of continuous integrable test functions is used to formulate the integral variational form of eq. (1.2) [Süli 2000]. A Fourier boundary condition is considered on the domain boundary $\partial\Omega$. The domain Ω is discretised using first-order linear simplexes defined

by their number of local nodes (denoted "NbLoc"): triangles in 2D with NbLoc=3 and tetrahedra in 3D with NbLoc=4. The outcome is a residual that we aim to minimize so that the conservation principle is satisfied. Therefore, the weak form writes:

$$\begin{aligned}&\forall \mathcal{W} \in M = \left\{u \in \mathcal{H}^1(\Omega)\right\}\\&\int_\Omega \mathcal{W}\frac{\partial\langle\rho h\rangle}{\partial t}\,\mathrm{d}V + \int_\Omega \mathcal{W}\langle\vec{v^l}\rangle\cdot\vec{\nabla}\left(\rho^l h^l\right)\,\mathrm{d}V - \int_\Omega \mathcal{W}\nabla\cdot\left(\langle\kappa\rangle\vec{\nabla}T\right)\,\mathrm{d}V - \int_\Omega \mathcal{W}\langle\dot{Q}_V\rangle\,\mathrm{d}V = 0\end{aligned} \tag{1.4}$$

where we assumed a static solid phase and an incompressible liquid phase, which allowed recasting the second term of eq. (1.2) into $\langle\vec{v^l}\rangle\cdot\vec{\nabla}\left(\rho^l h^l\right)$. The steps for discretizing in time and space the previous equation are well detailed in some book references like Rappaz et al. [2003] and Dantzig et al. [2009]. As for enthalpy and temperature, they are spatially discretized in each simplex using interpolations functions $\mathcal{P}$, thus defining the nodal values H_j and T_j, respectively:

$$\langle\rho h\rangle = \sum_{j=1}^{\text{NbLoc}} \mathcal{P}_j H_j \tag{1.5}$$

$$T = \sum_{j=1}^{\text{NbLoc}} \mathcal{P}_j T_j \tag{1.6}$$

Note that H_j is a volumetric enthalpy. The Galerkin formulation gives the following expression for the residual contribution at a mesh node i for time step t in a local element Ω_E:

$$\begin{aligned}&\left(R_i^E\right)^t = \mathcal{M}_{ij}^E\left(H_j^t - H_j^{t-\Delta t}\right) + \mathcal{A}_{ij}^E T_j^t + \left(\mathcal{K}1_{ij}^E + \mathcal{K}2_{ij}^E\right) - \mathcal{F}_i^E - \mathcal{S}_i^E = 0\\&i,j : 1 \rightarrow \text{NbLoc}\end{aligned} \tag{1.7}$$

where the numerical contributions can be detailed as follows:

$$\textit{transient term:}\quad \mathcal{M}_{ij}^E = \int_{\Omega_E} \frac{1}{\Delta t}\mathcal{P}_i\mathcal{P}_j\,\mathrm{d}V \tag{1.8}$$

$$\textit{advection term:}\quad \mathcal{A}_{ij}^E = \int_{\Omega_E} \rho^l C_p^l \mathcal{P}_i\langle\vec{v^l}\rangle\cdot\vec{\nabla}\mathcal{P}_j\,\mathrm{d}V \tag{1.9}$$

$$\textit{diffusion term:}\quad \mathcal{K}1_{ij}^E = \int_{\Omega_E} \langle\kappa\rangle\vec{\nabla}\mathcal{P}_i\vec{\nabla}\mathcal{P}_j\,\mathrm{d}V \tag{1.10}$$

$$\textit{boundary condition term 1:}\quad \mathcal{K}2_{ij}^E = \int_{\partial\Omega_E} h_{\text{ext}}\mathcal{P}_i\mathcal{P}_j\,\mathrm{d}S \tag{1.11}$$

$$\textit{boundary condition term 2:}\quad \mathcal{F}_i^E = \int_{\partial\Omega_E} h_{\text{ext}}T_{\text{ext}}\mathcal{P}_i\,\mathrm{d}S \tag{1.12}$$

$$\textit{source term:}\quad \mathcal{S}_i^E = \int_{\Omega_E} \mathcal{P}_i\langle\dot{Q}_V\rangle\,\mathrm{d}V \tag{1.13}$$

The surface integrals $\mathcal{K}2_{ij}^E$ and $\mathcal{F}_i^E$ are related to a Fourier-type boundary condition, with h_{ext} as a coefficient of heat exchange and T_{ext} as the external temperature far from the boundary. The energy conservation principle is satisfied when the sum of the residual contributions coming from all the mesh elements is zero. In other words, the following global residual defined by the assembly of these contributions, should be minimized:

$$\begin{aligned}&(R_i)^t = \mathcal{M}_{ij}\left(H_j^t - H_j^{t-\Delta t}\right) + \mathcal{A}_{ij}T_j^t + \left(\mathcal{K}1_{ij} + \mathcal{K}2_{ij}\right)T_j^t - \mathcal{F}_i - \mathcal{S}_i = 0\\ &i,j : 1 \rightarrow \text{NbGlob}\end{aligned} \tag{1.14}$$

where the global tensors $\mathcal{M}_{ij}$, $\mathcal{A}_{ij}$, $\mathcal{K}1_{ij}$, $\mathcal{K}2_{ij}$, $\mathcal{F}_i$ and $\mathcal{S}_i$ contain respectively, after an assembly step, the contributions of the local matrices $\mathcal{M}_{ij}^E$, $\mathcal{A}_{ij}^E$, $\mathcal{K}1_{ij}^E$, $\mathcal{K}2_{ij}^E$, $\mathcal{F}_i^E$ and $\mathcal{S}_i^E$ from each discretised element in the domain Ω. Accordingly, the indices i and j refer to global node numbers, where the total number of nodes is denoted by "NbGlob". It is clear that the global residual inherits the dependence between enthalpy and temperature. This is shown in eq. (1.14) where the average volume enthalpy is a function of the temperature. It infers that this residual is a non-linear function; therefore minimizing it requires an iterative non-linear algorithm. Our choice settles on the Newton-Raphson method, known for its quadratic convergence speed. A solidification problem can induce severe non-linearities from the release of the latent heat (which itself is temperature-composition dependent) and the variations of the thermophysical properties of the alloy with respect to temperature and average composition. This algorithm could thus treat such variations. Considering the link between enthalpy and temperature, eq. (1.14) may be solved either for enthalpy or for temperature as a nodal unknown; hence both formulations are presented hereafter.

1.3.1 Enthalpy-based approach

The residual is re-written using a Taylor series expansion to the first order for a non-linear iteration (ν) :

$$(R_i)^{(\nu+1)} = (R_i)^{(\nu)} + \left(\frac{dR}{dH}\right)_{ij}^{(\nu)} \Delta H_j^{(\nu)} + \mathcal{O}\left(H_j^2\right) \tag{1.15}$$

Neglecting the second order terms, the suggested correction at each iteration in view of cancelling the residual and giving the new value $H_j^{(\nu)}$, is given by the linear system in eq. (1.16) relative to what we call a *Hsolver*:

$$\left(\frac{dR}{dH}\right)_{ij}^{(\nu)} \left(H_j^{(\nu+1)} - H_j^{(\nu)}\right) = -R_i^{(\nu)} \tag{1.16}$$

where $\frac{dR}{dH}$ is a global tangent matrix yielding the variations of the residual with respect to the enthalpy in the last iteration, $H_j^{(\nu)}$. If eq. (1.7) is considered, then the contribu-

tion of an element Ω_E writes:

$$\left(\frac{dR}{dH}\right)_{ij}^{(\nu)E} = \mathcal{M}_{ij}^{E} + \underbrace{\mathcal{A}_{ij}^{E}\left(\frac{dT}{dH}\right)_{j}^{(\nu)}}_{\text{no sum on } j} + \underbrace{\left(\mathcal{K}1_{ij}^{E} + \mathcal{K}2_{ij}^{E}\right)\left(\frac{dT}{dH}\right)_{j}^{(\nu)}}_{\text{no sum on } j} \tag{1.17}$$

Equation (1.17) is the core of the enthalpy-based solver. The resolution of eq. (1.16) then yields a new estimate of the vector of nodal enthalpies $H^{(\nu+1)}$, which are the only unknowns to be solved for. Once determined at iteration (ν), convergence tests are performed (refer to section

1.3.2 Temperature-based approach

Similarly to the Hsolver, the local residual is recast for a nonlinear iteration (ν), leading this time to an iterative temperature correction:

$$\left(\frac{dR}{dT}\right)_{ij}^{(\nu)}\left(T_j^{(\nu+1)} - T_j^{(\nu)}\right) = -R_i^{(\nu)} \tag{1.18}$$

where $\frac{dR}{dT}$ is a global tangent matrix yielding the variations of the residual with respect to temperature $T_j^{(\nu)}$ at the previous iteration. This solver will be referred to as *Tsolver*. The contribution of an element Ω_E to this tangent matrix is evaluated as:

$$\left[\left(\frac{dR}{dT}\right)_{ij}^{(\nu)}\right]^{E} = \mathcal{M}_{ij}^{E} + \underbrace{\mathcal{A}_{ij}^{E}\left(\frac{dH}{dT}\right)_{j}^{(\nu)}}_{\text{no sum on } j} + \underbrace{\left(\mathcal{K}1_{ij}^{E} + \mathcal{K}2_{ij}^{E}\right)\left(\frac{dH}{dT}\right)_{j}^{(\nu)}}_{\text{no sum on } j} \tag{1.19}$$

In contrast to the previous solver, eq. (1.19) is the core of the temperature-based solver. The resolution of eq. (1.18) then yields a new estimate of the vector of nodal temperatures $T^{(\nu+1)}$, which are the only unknowns to be solved for. Once updated for iteration (ν), convergence tests are performed (refer to section

1.3.3 Convergence

The previous two sections described the iterative resolution of the same discretised energy conservation by both Tsolver and Hsolver. However, in eqs. (1.17) and (1.19), an important term emerges from the tangent matrix evaluation describing the variations between temperature and enthalpy: $\frac{dH}{dT}$ (or $\frac{dT}{dH}$). This term invokes the previously mentioned temperature-enthalpy tabulations which depend on the alloy composition. Consequently, $\frac{dH}{dT}$ (or $\frac{dT}{dH}$) has a great influence on the convergence of the Tsolver (respectively the Hsolver). When eq. (1.16) or eq. (1.18) is solved at iteration (ν), this

term is written using a finite difference:

$$\textbf{Tsolver} \qquad \left(\frac{dH}{dT}\right)_j^{(\nu+1)} = \frac{\langle \rho h \rangle_j^{(\nu+1)} - \langle \rho h \rangle_j^{(\nu)}}{T_j^{(\nu+1)} - T_j^{(\nu)}} \tag{1.20}$$

$$\textbf{Hsolver} \qquad \left(\frac{dT}{dH}\right)_j^{(\nu+1)} = \frac{T_j^{(\nu+1)} - T_j^{(\nu)}}{\langle \rho h \rangle_j^{(\nu+1)} - \langle \rho h \rangle_j^{(\nu)}} \tag{1.21}$$

For the Tsolver, the enthalpy $\langle \rho h \rangle_j^{(\nu)}$ is needed to evaluate eq. (1.20). In contrast, the Hsolver requires the value of $T_j^{(\nu)}$ to evaluate the corresponding eq. (1.21). In both cases, the unknown is determined by the temperature-enthalpy relation. The indices next to the mentioned unknowns indicate that this relation is used for each iteration (ν) at each mesh node j, hence affecting the global resolution time between the two solvers. The Hsolver needs a *H2T* to evaluate $\frac{dT}{dH}$, whereas the Tsolver needs a *T2H* to evaluate $\frac{dH}{dT}$. The flowchart in **??** demonstrates the process. It can be seen that Tsolver uses solely *T2H* procedure and the thermodynamic tabulations to determine the enthalpy, hence the term $\frac{dH}{dT}$. On the other hand, Hsolver repeats the same procedure a finite number of times in order to determine a temperature output through *H2T* and use it to compute $\frac{dT}{dH}$. This algorithmic difference leverages the Tsolver in terms of computation time providing the same numerical accuracy while conserving the total system energy. Convergence tests are necessary at the end of each iteration of the

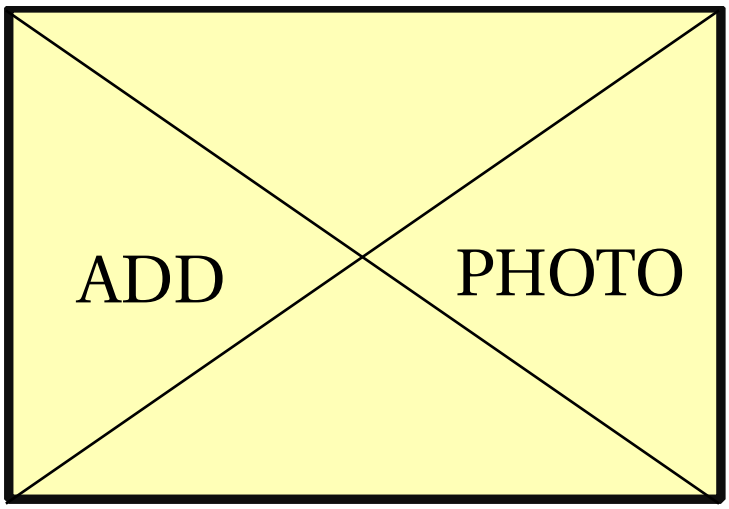

Fig. 1.1 – Flowcharts showing the steps to compute the nonlinear terms using tabulations

energy solver to determine the convergence status of the algorithm. In the context of the Tsolver for instance, the residual is re-evaluated with the newly determined

temperature $T_j^{(\nu+1)}$ and enthalpy $H_j^{(\nu+1)}$ so eq. (1.14) rewrites:

$$(R_i)^{(\nu+1)} = \mathcal{M}_{ij}\left(H_j^{(\nu+1)}) - H_j^{t-\Delta t}\right) + \mathcal{A}_{ij}T_j^{(\nu+1)} + (\mathcal{K}1_{ij} + \mathcal{K}2_{ij})\,T_j^{(\nu+1)} - \mathcal{F}_i - \mathcal{S}_i$$
$$i, j : 1 \rightarrow \text{NbGlob} \tag{1.22}$$

The norm of the current residual, $\|R^{(\nu+1)}\|$, is compared to a fixed small value $\varepsilon_R \approx \left[10^{-5}; 10^{-4}\right]$. The resulting temperature variation, $\left|T_j^{(\nu)} - T_j^{(\nu-1)}\right|$, should also respond to similar criterion between two consecutive iterations. For that purpose, we compare it to another fixed value $\varepsilon_T \approx \left[10^{-3}; 10^{-2}\right]$. Convergence is ultimately achieved when the following criteria are simultaneously met:

$$\begin{cases} \|R^{(\nu)}\| < \varepsilon_R \\ \text{Max}_{j:1\rightarrow\text{NbGlob}} \left|T_j^{(\nu)} - T_j^{(\nu-1)}\right| < \varepsilon_T \end{cases} \tag{1.23}$$

A comparison of both solver formulations is done in the hereafter test cases section.

1.4 Validation

1.4.1 Pure diffusion

The two solvers are first tested in a purely diffusive case for a one-dimensional solidification configuration. Predictions with a 1D front tracking model [Gandin 2000] is used as a benchmark. It provides solutions for the temperature and solid fraction during directional solidification of a 10 cm long Al – 7 wt.% Si ingot. The melt, with initial uniform temperature, is cooled with a heat exchange coefficient (assuming a Fourier boundary condition) from one side, the other side being adiabatic. All values for alloy properties, initial and boundary conditions and numerical parameters are listed in Table 1.2. For this simple test case, we use linear temperature dependence of the intrinsic phase enthalpies, that is $\langle\rho h\rangle^s = \langle\rho C_p\rangle T$ and $\langle\rho h\rangle^l = \langle\rho C_p\rangle T + \rho L$, where $\langle\rho C_p\rangle$ is the heat capacity per unit volume and ρL is the latent heat per unit volume. Values for $\langle\rho C_p\rangle$ and ρL, as well as for the thermal conductivities, $\kappa = \langle\kappa^l\rangle = \langle\kappa^s\rangle$, are taken constant. Moreover, a Gulliver Scheil approximation is used to compute a single temperature – fraction of solid relationship in the absence of macrosegregation. This is done assuming a linear binary phase diagram and thus requires using the properties listed in Table 1.2, i.e. the segregation coefficient, k, the liquidus slope, m_L, the liquidus temperature, T_L, and the eutectic temperature, T_E. Figures 1.3 and 1.4 show the comparison with the Hsolver and Tsolver. The results are found superimposed to the front tacking solution, thus giving validation of the implementation as well as the iterative schemes presented above to solve the energy conservation check table 1.2.

Initialisation

Time stepping	t, Δt
Nodal values	H_j^t, T_j^t, $(dH/dT)_j^t$

Newton-Raphson

Iteration step	$(\nu) = 0$
Nodal values	$H_j^{(\nu)} = H_j^t$,
	$T_j^{(\nu)} = T_j^t$,
	$(dH/dT)_j^{(\nu)} = (dH/dT)_j^t$

Local contributions

$\left[A^{(\nu)}\right]^E = \left[\left(\frac{dR}{dT}\right)_{ij}^{(\nu)}\right]^E$	(eq. (1.18))
$\left[b^{(\nu)}\right]^E = \left[R_j^{(\nu)}\right]^E$	(eq. (1.7))

Matrices assembly

Global matrices	$\left[A^{(\nu)}\right] \leftarrow \left[A^{(\nu)}\right]^E$, $\left[b^{(\nu)}\right] \leftarrow \left[b^{(\nu)}\right]^E$, $\forall E \in \Omega$
Residual norm	$\|R^{(\nu)}\| = \|A^{(\nu)}T^{(\nu)} - b^{(\nu)}\|$

Solve linear system $T^{(\nu+1)} = (A^{(\nu)})^{-1} b^{(\nu)}$

Microsegregation

Tabulation access	$\langle \rho h \rangle^{(\nu+1)} = \sum_\phi \left[g^\phi \rho^\phi h^\phi\right]_{T=T^{(\nu+1)}}$ (eq. (1.3))

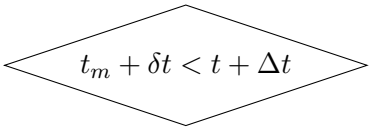

Fig. 1.2 – Resolution algorithm of the temperature-based solver.

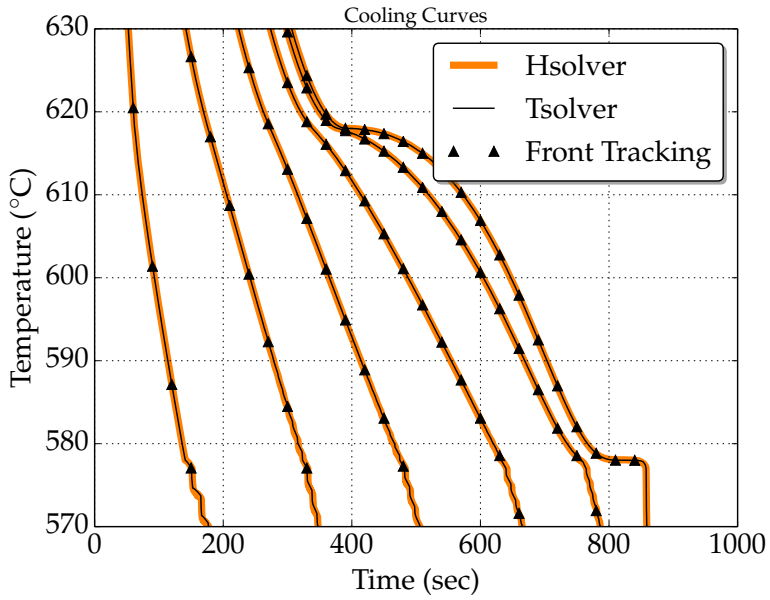

Fig. 1.3 – Computed unidirectional heat diffusion during solidification of an Al-7 wt.% Si alloy using (orange) the enthalpy method and (black) the temperature method, comparison being made for cooling curves. Each curve corresponds to a position along the sample, from 0 cm (cooling side) to 10 cm (insulated side), with 2 cm spacing between the positions.

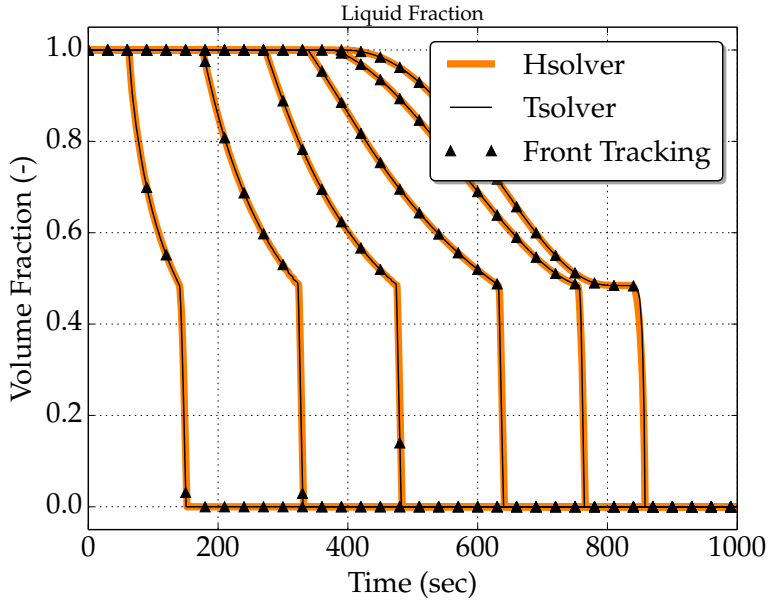

Fig. 1.4 – Computed unidirectional heat diffusion during solidification of an Al-7 wt.% Si alloy using (orange) the enthalpy method and (black) the temperature method, comparison being made for the liquid fraction history. Each curve corresponds to a position along the sample, from 0 cm (cooling side) to 10 cm (insulated side), with 2 cm spacing between the positions.

Table 1.2 – Parameters for the pure diffusion test case with alloyAl-7 wt.% Si presented in fig. 1.3

Parameter	Symbol	Value	Unit
Nominal composition	$\langle w \rangle_0$	7	wt.%
Liquidus temperature	T_L	618	°C
Eutectic temperature	T_E	577	°C
Segregation coefficient	k	0.13	–
Liquidus slope	m_L	–6.5	K wt.%$^{-1}$
Heat capacity (liquid and solid)	ρC_p	2.6×10^6	J m^{-3} K^{-1}
Enthalpy of fusion	ρL	9.5×10^8	J m^{-3}
Thermal conductivity (liquid and solid)	κ	70	W m^{-1} K^{-1}
Heat transfer coefficient	h_{ext}	500	W m^{-2} K^{-1}
External temperature	T_{ext}	100	°C
Initial temperature	T_0	800	°C
Ingot length		0.1	m
FE mesh size		10^{-3}	m
Time step	Δt	0.1	s
Convergence criterion (residual)	ε_R	10^{-6}	–
Convergence criterion (temperature)	ε_T	10^{-2}	K

1.4.2 Convection-diffusion with macrosegregation

Conservation equations in **Table 2** are for mass, momentum and chemical species. As for energy, they are presented after the volume averaging technique has been applied [Ni et al. 1991; Dantzig et al. 2009]. Moreover, an assumption of a static and non deformable solid phase is made. Consequently, the mechanical model is reduced to the conservation of momentum in the liquid phase. This assumption also yields some other consequences on the mass balance and the liquid momentum conservation. In the latter, a Darcy term is added to take into account the dissipative interfacial stress in the porous-like mushy zone. Its main parameter is the permeability of the mushy zone, K. It is considered isotropic, hence reducing to a scalar which is given by the Carman-Kozeny relation, based on the secondary dendrite arm spacing λ_2 : $K = \frac{{g^l}^3 \lambda_2^2}{180\left(1-g^l\right)^2}$. The liquid density being taken constant, its spatial variations as a function of temperature and average composition are still needed to compute thermosolutal convection forces. For that purpose, the Boussinesq approximation $\langle \rho \rangle^l = \rho_{\text{ref}} \left(1 - \beta_T \left(T - T_0\right) - \beta_{\langle w \rangle^l} \left(\langle w \rangle^l - w_0^l\right)\right)$ is used, considering the thermal β_T and solutal $\beta_{\langle w \rangle^l}$) expansion coefficients and a reference density, ρ_{ref}, defined at a reference temperature T_0 and reference composition w_0^l. Values for the references are taken at the liquidus temperature and the nominal composition of the alloy, $\langle w \rangle_0$

[Carozzani et al. 2013]. More details about the FE formulation can be found in the Ph.D work of Rivaux [2011] and Carozzani [2012]. It should be noted that the macroscopic solute diffusion coefficient in the solid phase is neglected in **REF Eq. 15c**.

in this table I use directly the simplified equations, but this was done only for the article, now I have to go from the full conservation equations and state the hypothesis and methods that i used to reach this simplified form

$$\nabla \cdot \left(g^l \vec{v^l} \right) = 0 \tag{1.24a}$$

$$\frac{\partial}{\partial t}\left(g^l \rho_{\text{ref}} \vec{v^l} \right) + \vec{\nabla} \cdot \left(g^l \rho_{\text{ref}} \vec{v^l} \times \vec{v^l} \right) - \vec{\nabla} \cdot \langle S \rangle^l - g^l \nabla p^l + \mu^l {g^l}^2 K^{-1} \vec{v^l} - g^l \rho^l \vec{g} = 0 \tag{1.24b}$$

$$\frac{\partial}{\partial t}\left(\langle w_i \rangle \right) + \left(g^l \vec{v^l} \right) \cdot \vec{\nabla} w_i^l + \nabla \cdot \left(g^l D^l \vec{\nabla} w_i^l \right) = 0 \tag{1.24c}$$

Table 1.3 – Averaged conservation equations for the conservation of mass (a), momentum (b) and solute mass (c)

Figure SMACS: Computed unidirectional heat diffusion during solidification of an Al-7 wt.% Si alloy using (orange) the enthalpy method and (black) the temperature method, comparison being made for (left) cooling curves and (right) time history of the liquid fraction. Each curve corresponds to a position along the sample, from 0 cm (cooling side) to 10 cm (insulated side), with 2 cm spacing between the positions.

The Tsolver's ability to be coupled with various physical phenomena like macrosegregation and fluid flow in porous medium is displayed in this test case. It consists of a solidification benchmark where a 10 cm width $\times$ 6 cm height $\times$ 1 cm thick cavity containing a Sn-3 wt.% Pb melt is cooled down from its two narrowest vertical sides using heat exchangers (LHE: left heat exchanger, RHE: right heat exchanger). The experiment, inspired by Hebditch et al. [1974] similar set up, has been revisited by Hachani et al. [2012] who performed the solidification with better controlled conditions and using an increased number of samples for composition analysis. Recently, a successful attempt to simulate the experiment was carried out by Carozzani et al. [2013] relying on an enthalpy resolution. All details regarding geometry, finite element discretization, material properties and boundary conditions can be found in the latter reference.

I could develop more here giving additional details

For this computation, solidification paths, phase compositions and phase enthalpies were determined by a thermodynamic module dedicated to equilibrium calculations for binary alloys. The 3D simulation results in **REF Figure 4** show a satisfactory agreement with the experimental temperature measurements recorded at mid heights of the cavity and uniformly distributed along its width [Carozzani et al. 2013]. In fact, simulation results with the Tsolver and the Hsolver were found to be almost superimposed, as in **REF Figure 4**. Regarding the computation, the Tsolver resolution proves

to be faster than the Hsolver used by Carozzani et al. [2013]: a process time of 7000s required a computation time of 90 hours 13 minutes compared to 114 hours 21 minutes spent by the enthalpy resolution with 32 cores on the same cluster. The gain factor is about 20%.

Bibliography

[Bellet et al. 2009]
Bellet, M. et al. (2009). "Call for contributions to a numerical benchmark problem for 2D columnar solidification of binary alloys". *International Journal of Thermal Sciences,* 48 (11), pp. 2013–2016. URL: http://www.sciencedirect.com/science/article/pii/S129007290900177X (cited on page 2).

[Carozzani 2012]
Carozzani, T. (2012). "Développement d'un modèle 3D Automate Cellulaire-Éléments Finis (CAFE) parallèle pour la prédiction de structures de grains lors de la solidification d'alliages métalliques". PhD thesis. Ecole Nationale Supérieure des Mines de Paris. URL: http://pastel.archives-ouvertes.fr/pastel-00803282 (cited on page 14).

[Carozzani et al. 2013]
Carozzani, T. et al. (2013). "Direct Simulation of a Solidification Benchmark Experiment". *Metallurgical and Materials Transactions A,* 44 (2), pp. 873–887. URL: http://link.springer.com/article/10.1007/s11661-012-1465-1 (cited on pages 2, 14, 15).

[Dantzig et al. 2009]
Dantzig, J. A. and Rappaz, M. (2009). *Solidification.* EPFL Press (cited on pages 6, 13).

[Doré et al. 2000]
Doré, X., Combeau, H., and Rappaz, M. (2000). "Modelling of microsegregation in ternary alloys: Application to the solidification of Al–Mg–Si". *Acta Materialia,* 48 (15), pp. 3951–3962. URL: http://www.sciencedirect.com/science/article/pii/S1359645400001774 (cited on page 2).

[Du et al. 2007]
Du, Q., Eskin, D. G., and Katgerman, L. (2007). "Modeling Macrosegregation during Direct-Chill Casting of Multicomponent Aluminum Alloys". *Metallurgical and Materials Transactions A,* 38 (1), pp. 180–189. URL: http://link.springer.com/article/10.1007/s11661-006-9042-0 (cited on page 2).

[Gandin 2000]
Gandin, C. A. (2000). "From constrained to unconstrained growth during directional solidification". *Acta Materialia,* 48 (10), pp. 2483–2501. URL: http://www.sciencedirect.com/science/article/pii/S1359645400000707 (cited on page 10).

[Hachani et al. 2012]
Hachani, L. et al. (2012). "Experimental analysis of the solidification of Sn–3 wt.%Pb al-

loy under natural convection". *International Journal of Heat and Mass Transfer*, 55 (7–8), pp. 1986–1996. URL: http://www.sciencedirect.com/science/article/pii/S0017931011007009 (cited on page 14).

[**Hebditch et al. 1974**]
Hebditch, D. J. and Hunt, J. D. (1974). "Observations of ingot macrosegregation on model systems". *Metallurgical Transactions*, 5 (7), pp. 1557–1564. URL: http://link.springer.com/article/10.1007/BF02646326 (cited on page 14).

[**Ni et al. 1991**]
Ni, J. and Beckermann, C. (1991). "A volume-averaged two-phase model for transport phenomena during solidification". *Metallurgical Transactions B*, 22 (3), pp. 349–361. URL: http://link.springer.com/article/10.1007/BF02651234 (cited on pages 3, 13).

[**Rappaz et al. 2003**]
Rappaz, M., Bellet, M., and Deville, M. (2003). *Numerical Modeling in Materials Science and Engineering*. Springer Series in Computational Mathematics. Springer Berlin Heidelberg (cited on pages 3, 6).

[**Rivaux 2011**]
Rivaux, B. (2011). "Simulation 3D éléments finis des macroségrégations en peau induites par déformations thermomécaniques lors de la solidification d'alliages métalliques". PhD thesis. École Nationale Supérieure des Mines de Paris. URL: http://pastel.archives-ouvertes.fr/pastel-00637168 (cited on page 14).

[**Süli 2000**]
Süli, E. (2000). *Lecture Notes on Finite Element Methods for Partial Differential Equations* (cited on page 5).

[**Swaminathan. et al. 1993**]
Swaminathan., C. R. and Voller, V. R. (1993). "On The Enthalpy Method". *International Journal of Numerical Methods for Heat & Fluid Flow*, 3 (3), pp. 233–244. URL: http://www.emeraldinsight.com/journals.htm?articleid=1665561&show=abstract (cited on page 2).

[**Thuinet et al. 2004**]
Thuinet, L. and Combeau, H. (2004). "Prediction of macrosegregation during the solidification involving a peritectic transformation for multicomponent steels". *Journal of Materials Science*, 39 (24), pp. 7213–7219. URL: http://link.springer.com/article/10.1023/B%3AJMSC.0000048734.34597.1e (cited on page 2).